Cellulose (2013) 20:1911–1923
DOI 10.1007/s10570-013-9952-0

ORIGINAL PAPER

Effect of microcrystal cellulose and cellulose whisker on biocompatibility of cellulose-based electrospun scaffolds

Baoquan Jia · Yutao Li · Bin Yang · Di Xiao · Shengnan Zhang · A. Varada Rajulu · Tetsuo Kondo · Lina Zhang · Jinping Zhou

Received: 21 February 2013 / Accepted: 14 May 2013 / Published online: 23 May 2013

Abstract To investigate the potential application of microcrystal cellulose (MCC) and cellulose whisker (CW) in the electrospun vascular tissue scaffolds, cellulose acetate (CA) and cellulose composite scaffolds containing MCC and CW were electrospun from CA solutions and deacetylation. Structure and morphology of MCC, CW and the fibrous composite scaffolds were investigated using FT-IR, SEM, TEM and AFM. The wettability of the scaffolds was evaluated by water contact angle analysis. The effect of MCC and CW on the biocompatibility of the scaffolds for vascular smooth muscle cells (VSMC) was assayed by MTT test, fluorescent imaging and SEM. The biocomposite scaffolds displayed multi-scaled structure and morphology. The scaffolds containing MCC and CW simultaneously exhibited significantly higher cell viability compared to those with only MCC or CW and no filler. Cell viability and morphology within the scaffolds become better with increasing content of MCC and CW. The composite scaffolds with both micro- and nano-scale organization could mimic the native extracellular matrix more closely, and further produce synergistic enhancement on VSMC viability, adhesion and proliferation. This study provides the potential applications of renewable cellulose-based particulates in biomedical field.

Keywords Microcrystal cellulose · Cellulose whisker · Biocomposite scaffold · Biocompatibility · Tissue engineering

Electronic supplementary material The online version of this article (doi:10.1007/s10570-013-9952-0) contains supplementary material, which is available to authorized users.

B. Jia · Y. Li · B. Yang · S. Zhang · L. Zhang · J. Zhou (✉)
Department of Chemistry, Wuhan University, Wuhan 430072, China
e-mail: zhoujp325@whu.edu.cn

D. Xiao
School of Land and Environment, University of Melbourne, Melbourne 3010, Australia

A. V. Rajulu
Department of Polymer Science and Technology, Sri Krishnadevaraya University, Anantapur 515 055, India

T. Kondo · J. Zhou
Graduate School of Bioresource and Bioenvironmental Sciences, Kyushu University, 6-10-1, Hakozaki, Higashi-ku, Fukuoka 812-8581, Japan

Introduction

Providing a suitable scaffold for the extracellular matrix (ECM) is very important in tissue engineering, and various techniques have been applied to fabricate tissue scaffolds (Zhu et al. 2004; Hoffman 2012; Thibault et al. 2013). Electrospinning is considered as a promising method, because the high surface area and porous structure of the as-spun scaffolds are of great benefit to tissue engineering and the continuous fiber is

also helpful to cellular interactions (Ladd et al. 2011; Rnjak-Kovacina et al. 2011; Coburn et al. 2012). Advantages of electrospinning also include that the morphology of fiber and the shape of the scaffold can be tailored by changing relevant processing variables and different electrospinning method, respectively (Deitzel et al. 2001; Teo et al. 2005). However, biomaterial activity is still one key factor in designing an artificial bioscaffold (Kakisis et al. 2005). To achieve that aim, numerous methods have been carried out (Ma et al. 2005; Gouma et al. 2010; Wu et al. 2011; Truong et al. 2012; Wang et al. 2012). Among these methods, loading specific particulates was thought to be a facile one.

Natural biopolymers, such as cellulose, chitosan and collagen, show superiority over synthetic polymers as promising candidates due to their inherent better biocompatibility (Khademhosseini et al. 2006; Van Vlierberghe et al. 2011). As the most abundant natural polymer, cellulose and cellulose based materials are intriguing for the huge biomass production and ecological-friendly properties (Klemm et al. 2005). The remarkable mechanical performance, physiological inertness and biocompatibility of cellulosic materials have been attracted many attentions to the potential application in tissue engineering (Müller et al. 2006; Bhattacharya et al. 2012; Rodríguez et al. 2012). Microcrystal cellulose (MCC) and cellulose whisker (CW) are the micro- and nano-scale particulates of cellulose, respectively. They are usually prepared through mechanical treatment or acid hydrolysis of bulk cellulose (Araki et al. 1998; Chakraborty et al. 2005; Li et al. 2011; Shopsowitz et al. 2011). MCC has been widely used for a long time as additive and binder in pharmaceuticals, food, cosmetics and environmentally friendly biocomposites (Das et al. 2009; Eldessouki et al. 2011). CW brings about substantial research on fabricating materials from renewable resources owing to the dramatic mechanical improvement for the nanocomposite material (Favier et al. 1995). The recent research reveals that CW has no evident cytotoxicity and low nonspecific cellular uptake (Dong et al. 2012). And oriented whiskers can regulate the morphology and differentiation of skeletal muscle cells, meanwhile promoted skeletal muscle myogenesis (Dugan et al. 2010, 2013). Potential applications of CW extend likewise to biomedical implants, drug delivery, flexible displays and so on (Moon et al. 2011). It is reported that the electrospun cellulose acetate (CA) nanocomposite scaffold containing low amount of CW exhibits significantly improved mechanical property at body temperature (Pooyan et al. 2012). However, how NCC affect the biocompatibility of the CA composite scaffolds has not been mentioned. Materials which are organized on multiple scales have been found to show more resemblance to biological matrices than those with single scale, and usually provide beneficial effects (Tuzlakoglu et al. 2005; Zhao et al. 2010). Due to the different size scales of MCC and CW, it is of much interest to investigate the combined effect of MCC and CW. In order to better understand the effects of the different sized particulates, CA was used as the fibrous matrix. Electrospinning CA is much easier than electrospinning cellulose, and the CA scaffolds can be easily hydrolyzed into cellulose (Liu and Hsieh 2002; Son et al. 2004a, b; Du and Hsieh 2009), so the difference in the inherent biocompatibility could be excluded.

In this work, all cellulose-based composite scaffolds containing MCC and CW were prepared through electrospinning. The morphology, structure and properties of the composite scaffolds were investigated with FT-IR, SEM, TEM and water contact angle analysis. The synergistic effects of MCC and CW on the VSMC viability and adhesion within the fibrous scaffolds have been interpreted. With the physiological inertness and inherent biocompatibility, MCC and CW are probably suitable additives to improve the biocompatibility of vascular scaffolds.

Experimental

Materials

Cellulose acetate with 54.5–56.0 % combination of acetyl content was purchased from Sinopharm Chemical Reagent Co. Ltd., China. MCC PH-101 with DP 100–130 was bought from Asahi Kasei Chemicals Corporation (Japan). Cotton linter pulp was provided by Hubei Golden Ring Co., Ltd. (Xiangyang, China). 3-[4,5-dimethylthiazol-2-yl]-2,5-diphenyltetra-zoliumbromide (MTT) was purchased from Invitrogen Corp (USA).

Table 1 Component, filler content, diameter distribution, contact angle and porosity of the CA composite electrospun scaffolds

Code	Component	Filler content[a] (%)	Diameter (Mean ± SD) (nm)	Contact angle (Mean ± SD) (°)	Porosity (Mean ± SD) (%)
S1	CA	0	1,043 ± 470	105.4 ± 2.0	53.4 ± 7.4
S2	CA/MCC	5	982 ± 558	98.5 ± 0.7	73.7 ± 3.1
S3	CA/CW	5	954 ± 336	101.0 ± 1.4	60.7 ± 7.1
S4	CA/MCC/CW[b]	5	1,214 ± 517	100.3 ± 0.7	72.2 ± 8.2
S5	CA/MCC/CW[b]	7.5	1,113 ± 541	98.8 ± 3.0	69.3 ± 7.1
S6	CA/MCC/CW[b]	10	1,016 ± 572	98.0 ± 2.7	79.7 ± 8.8

[a] The filler content of CA composite electrospun scaffolds

[b] MCC:CW = 1:1 by weight

Preparation of MCC and CW

Microcrystal cellulose was prepared as following. PH-101 (20 g) was treated with 50 wt% H_2SO_4 (100 mL) for 5 h at 60 °C. Then 1 L water was poured to finish the reaction, and the obtained suspension was centrifugated for 6–7 times at 7,200 rpm. The supernatant was decanted after centrifugation, and deionized water was added to wash residual acid and soluble hydrolysates. Finally, the residue was dialyzed against deionized water, and the suspension was frozen and lyophilized.

Cellulose whisker was prepared according to the previous methods (Shopsowitz et al. 2011). The cotton linter pulp was first crushed in a cryo-pulverizer. Afterwards, 4 g crushed pulp was put in 35 mL 64 wt% H_2SO_4 and vigorously stirred at 45 °C for 25 min. The suspension was diluted with 400 mL cold deionized water to cease the hydrolysis and allowed to settle overnight. The clear top layer was decanted, and the cloudy suspension was centrifuged at 7,200 rpm for 3 times to remove acid and soluble hydrolyzates. The collected suspension was dialyzed against deionized water and freeze-dried.

Preparation of CA composite electrospun scaffolds

Cellulose acetate solution (10 wt%) was prepared (Son et al. 2004b) by dissolving CA in a mixed solvent of acetone/water (80:20, w/w). MCC and CW were dispersed in CA solution with ultrasonication for 45 min, and the solid content was fixed to 10 wt%. The suspensions were delivered at a constant flow rate of 3 mL/h for electrospinning with a precision pump (Longer Precision Pump Co., Ltd., China). The applied potential was 12 kV (Dongwen High Voltage Power Supply, China) and the working distance between the needle tip and the aluminum foil was 12 cm. According to Table 1, six CA composite electrospun scaffolds were prepared.

Deacetylation of the composite electrospun scaffolds

Cellulose acetate composite electrospun scaffolds were fixed in nylon mesh envelopes and then immersed in 0.05 M NaOH/ethanol solution for 3 h. The fibrous scaffolds were shaken during the hydrolysis process. Then the fibrous mats were washed with ethanol and water for three times. The hydrolyzed scaffolds were air-dried at 50 °C and coded as S1′–S6′ corresponding to the original CA composites S1–S6.

Cell culture and MTT assay

Wistar rat aortic vascular smooth muscle cells (VSMC) were cultured in 50 mL cell culture flask with DMEM/F 12 (Gibco), supplemented with 10 % fetal bovine serum, 100 U/mL penicillin, streptomycin and 2 % glutamine. Cell culture was maintained in a gas-jacket incubator equilibrated with 5 % CO_2 at 37 °C. When the cells had grown to confluence, they were digested by 2 mL 0.25 % trypsin (Sigma) for 1–2 min, and then 5 mL culture medium was added to stop digestion. The culture medium was aspirated to get cells dispersed and counted.

The scaffolds were punched into small wafers (6 mm in diameter) in order to locate the disks into the 48-well tissue culture plate. After sterilization of the

wafers with 75 % ethanol and 30 min exposure under UV light, 200 μL (ca. 5×10^4 cells/mL) of cell dispersion was placed on the wafers and cultured for 24 h. The viability and proliferation of VSMC were determined by MTT assay. Then the original culture medium was removed with a macro-pipette and 200 mL of fresh culture medium was added to each well. 20 μL of MTT solution (5 mg/mL) was added to the culture well incubated at 37 °C and 5 % CO_2 for 4 h. The upper medium was removed carefully and the intracellular formazan was solubilized by adding 500 μL of DMSO to each well. The absorbance of produced formazan was measured at 570 nm with a Microplate Reader Bio-Rad 5 50 (Hercules, USA). The standard curve of absorbance versus cell number within every well was measured (Fig. S1). The cell viabilities were calculated by the following formula:

$$Cell\ viability = \frac{OD_{Sample} - OD_{Blank}}{OD_{Control} - OD_{Blank}} \times 100\ \%$$

Three wafers were applied for each sample. Statistical analyses were performed using the two-tailed t test assuming equal variance for two samples. Differences were considered statistically significant at $P < 0.05$.

Characterization

Flourier transformed infrared spectroscopy (FT-IR) was recorded on Thermo iS10 spectrometer. The scaffolds were first cut into powders and dried in vacuum at 50 °C before FT-IR measurement. Water contact angles were measured on a drop shape analysis system (DSA100, KRÜSS, Germany). The picture was taken immediately when the water dripped onto the scaffold surface. The number of tested pieces for each sample is 3.

Morphology of the electrospun scaffolds, MCC and cell situation within the electrospun scaffolds were observed on QUANTA scanning electron microscope (FEI Co., Eindhoven, The Netherlands) and Sirion 200 field emission SEM (FEI Co., Eindhoven, The Netherlands). For the biological samples, cells were first cultivated for 2 days, and then the wafers were rinsed with PBS for three times and fixed in 4 % of

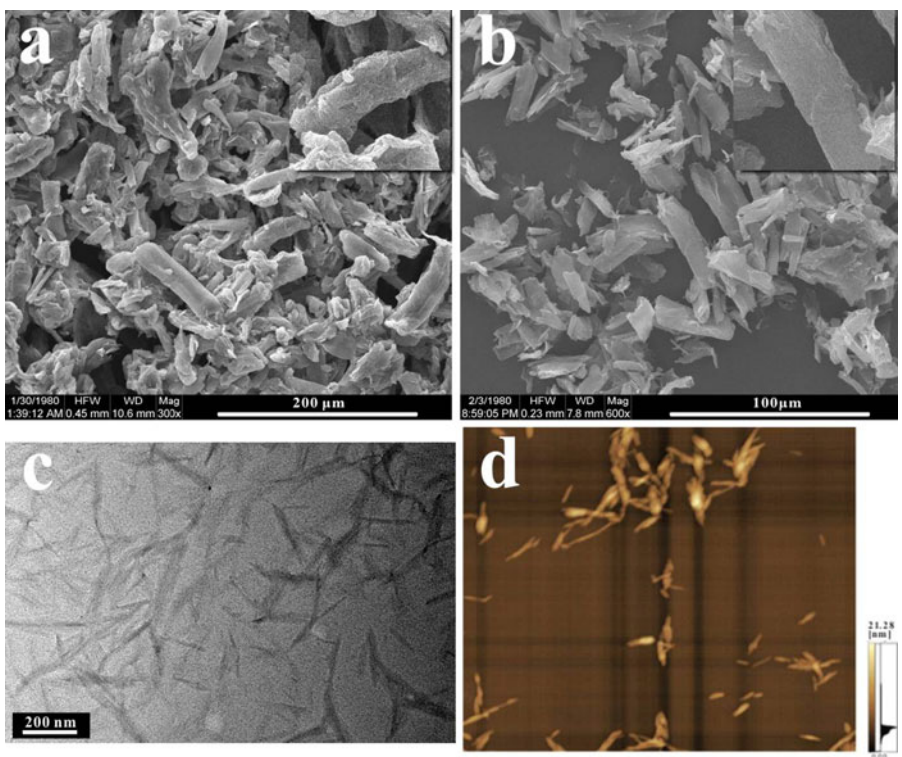

Fig. 1 SEM images of **a** PH-101 and **b** MCC after acid degradation, **c** TEM micrograph of CW, and **d** AFM image of CW (2 μm × 2 μm)

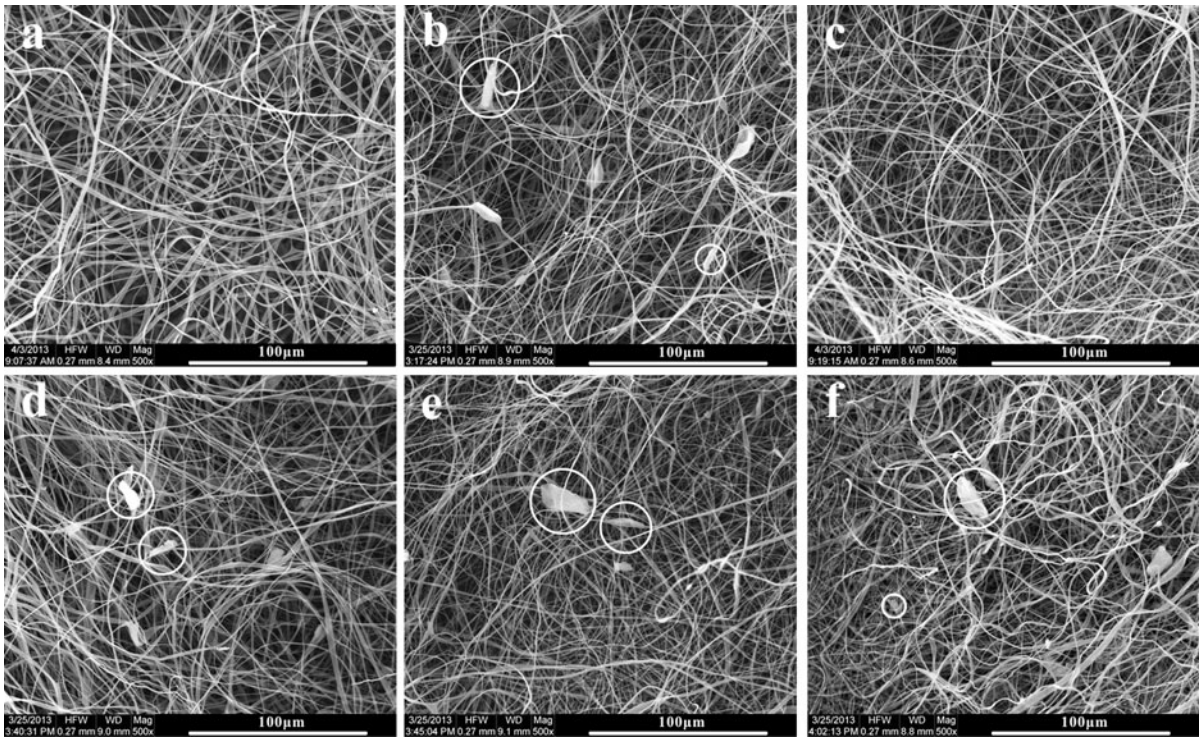

Fig. 2 SEM images of **a** S1, **b** S2, **c** S3, **d** S4, **e** S5 and **f** S6. The presence of MCC was marked by *white circle*

formaldehyde/PBS solution overnight. Afterwards, they were rinsed with PBS and dehydrated with a series of graded ethanol solutions. Freeze-drying was employed for maintaining the cell morphology. All the wafers were sputtered with gold before taking SEM images. The sizes of MCC, CW and electrospun fibers were measured with the aid of software (ImageJ).

To calculate the porosity of the scaffolds, the wet weight (W_w) was obtained after immersing the scaffold in water for 24 h. And the dry weight (W_d) was measure after drying at 50 °C for 24 h. Porosity of the scaffold was calculated by the equation:

$$Porosity = \frac{(W_w - W_d)}{V_s} \times 100\ \%$$

where V_s stands for the measured volume of the scaffold.

Transmission electron microscopy (TEM) images of CW and S6 were acquired on a JEM-2100 transmission electron microscope (JEOL Ltd., Japan). The suspension of CW (0.05 wt%) was prepared by ultrasonic dispersion. The suspension was dripped onto the copper grid and air-dried. Atomic force microscopy (AFM) was performed on a scanning probe microscope (SPM-9500J3, Shimadzu, Japan) with tapping mode. The suspension of CW was added onto a freshly cleaved mica plate and air-dried overnight. Fluorescent micrographs were obtained after the VSMC were cultured for 2 days and stained with calcein-AM, 4,6-diamidino-2-phenylindole (DAPI) and propidium iodide (PI) dyes were performed on a microscope equipped with a colored CCD camera (Axiovert 200M, Carl Zeiss, Germany).

Results and discussion

Morphology of MCC and CW

Figure 1a, b show the SEM images of PH-101 and the hydrolyzed MCC, respectively. The stock powder (PH-101) has a size about 100 μm length and 20 μm width (Fig. 1a). The dimension was too large to prepare the fibrous composite scaffolds considering the dimension of electrospun fiber. After acid treatment, smaller particles with a size of 19 ± 9 μm length and 5 ± 2 μm width were obtained (Fig. 1b). The acid-treated MCC maintained the original

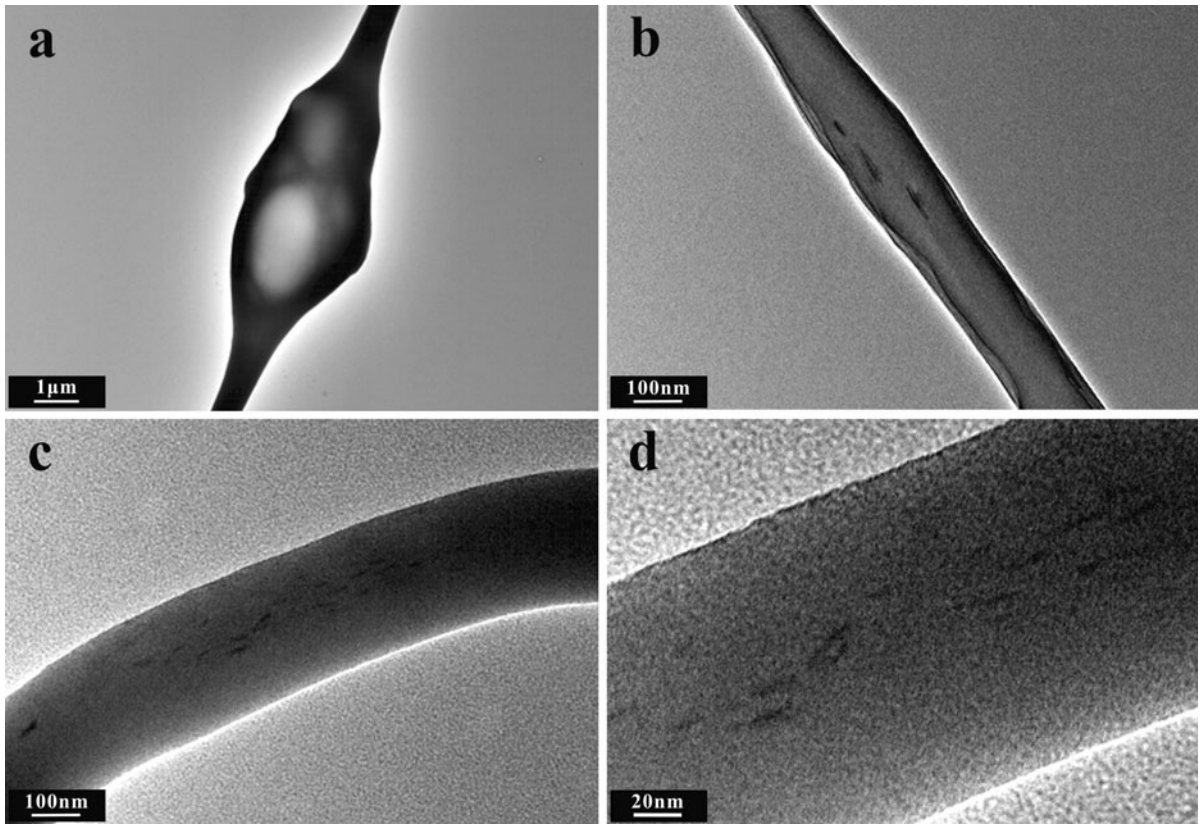

Fig. 3 TEM images of the CA composite scaffold (S6) with MCC and CW content of 10 wt%

rod-like morphology of PH-101. The surface was also smoothened by acid etching process. CW prepared from cotton linter exhibits needle-like shape, which can be observed clearly using TEM and AFM (Fig. 1c, d). The whisker has a diameter of 10 ± 2 nm and the length of 156 ± 47 nm measured from the TEM image.

Structure and properties of the electrospun scaffolds

Figure 2 shows the SEM images of the CA composite electrospun mats. Decoration of MCC on fibers could be observed in the images due to the micro-scale dimension, which surely increased the roughness of fibers. But CW had little influence on the fiber surface morphology owing to its small dimension. To summarize the diameter distribution, 100 fibers were counted randomly and measured. The data are displayed in Fig. S2 and Table 1. The diameters of the fibers were at submicro-range. Scaffolds containing MCC had a broadened fiber distribution, due to the unstable jet flow caused by the unbalanced forces among the surface tension, viscoelastic, and electrostatic forces caused by the micro-scaled particles (Zhou et al. 2011). Some secondary fibers (100–300 nm) were arisen from the surface (Fig. S3). As listed in Table 1, blending MCC and CW (especially MCC) increased the porosity of the scaffolds. Sulfuric acid hydrolyzed CW was usually negatively charged by sulfate ester. The charged particles could increase the conductivity of the solution, thus stabilize the electrospinning process. Therefore, S3 displayed more uniform fiber distribution than the others.

Figure 3 shows the TEM images of S6. Based on the shape and size, MCC could be seen located along the fiber (Fig. 3a). CW was observed by the different contrast from CA matrix (Zhou et al. 2011). As shown in Fig. 3b–d, the whiskers dispersed along the fibers, part of them was wrapped by CA matrix and could not be observed clearly. According to the size of MCC,

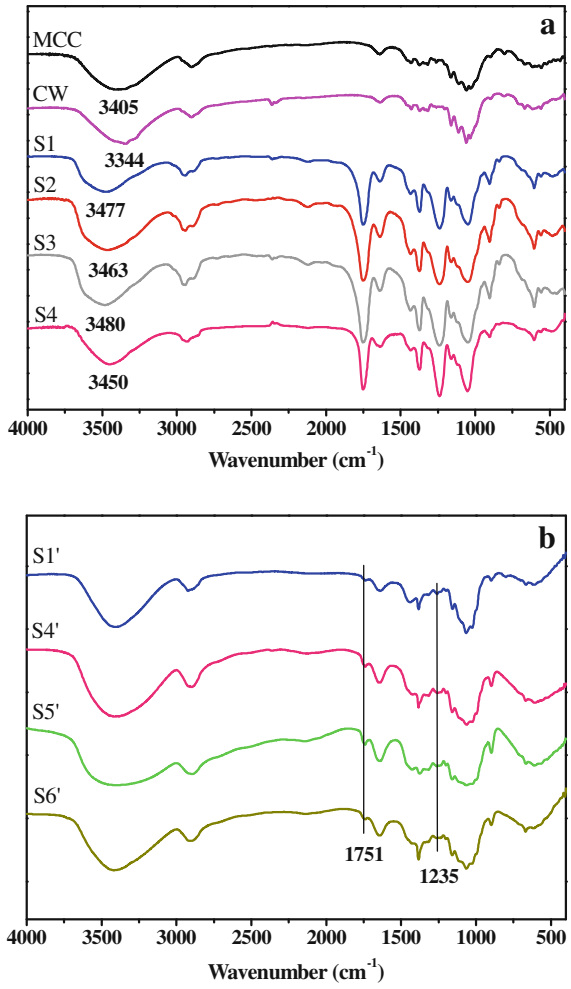

Fig. 4 FT-IR spectra of **a** MCC, CW and the CA composite scaffolds (S1–S6), and **b** the deacetylated cellulose composite scaffolds (S1′, S4′–S6′)

electrospun fiber and CW, the biocomposite scaffolds with MCC and CW possessed multi-scaled feature.

Figure 4a illustrates the FT-IR spectra of the CA composite scaffolds. Peaks at 1,751 and 1,235 cm^{-1} are assigned to the C=O and C–O vibrating mode of carboxylate group (Ilharco and de Barros 2000). The bands at 3,405, 3,344, 3,477, 3,463, 3,480 and 3,450 cm^{-1} are attributed to stretching vibration modes of O–H groups of MCC, CW, S1, S2, S3, and S4, respectively. The O–H stretching vibration of CW is located at lower wavenumber than MCC, because the H-bonding interaction of CW is stronger than MCC owing to the large specific area (Watanabe et al. 2007). For the electrospun scaffolds, addition of MCC or CW alone has no significant influence over the H-bonding of the scaffolds.

Wettability of the electrospun scaffolds was analyzed by water contact angle, and the data are shown in Fig. 5 and Table 1. Water contact angles of MCC and CW are 51.0 ± 0.9° and 36.2 ± 2.1°, respectively. The biocomposite scaffolds exhibited lower angles than CA ones. However, the water contact angle of S2 was lower than S3. As a result of the large size, MCC was more inclined to change the fiber surface morphology and stay uncovered. CW was too small to change the surface morphology; in addition, many of whiskers were wrapped inside the fiber. Thus, the electrospun scaffolds containing MCC exhibited more hydrophilic than CW. The contact angles of the scaffolds decreased as the content of MCC increased, and it also suggested MCC showed more obvious influence over the fiber surface.

Cell viability and proliferation of the CA composite scaffolds

Microcrystal cellulose has been commercially used as an additive in food and pharmaceuticals. CW, as reported, has no obvious cytotoxicity (Dong et al. 2012; Male et al. 2012). Dugan found the skeletal muscle cells was more motile on CW surfaces than the glass (Dugan et al. 2010). Figure 6 shows the effect of MCC and CW over the VSMC viability within the electrospun scaffolds assessed by MTT assay. The electrospun CA scaffold (S1) was not suitable for the cultivation of VSMC. Compared to S1, the cell viabilities of the scaffolds containing only MCC or CW (S2 and S3) were not significantly improved. Interestingly, through blending both MCC and CW into the CA matrix, the cell viability was obviously improved. Although the total content of fillers was the same as S2 and S3, the cell viability of S4 was significantly higher than S1 ($P < 0.05$). The cell viability of S5 and S6 was higher than S4 as a result of increasing additives content. For example, the cell viability of S6 was twofold higher than S1, and even better than the control group. The results suggested the CA composite scaffolds containing both MCC and CW exhibited noticeable improvement of biocompatibility.

Figure 7 shows the situation of cell attachment and morphology within the electrospun scaffolds examined through fluorescent microscope imaging. The dead cells and cell nuclei within S1, S4 and S6 were also

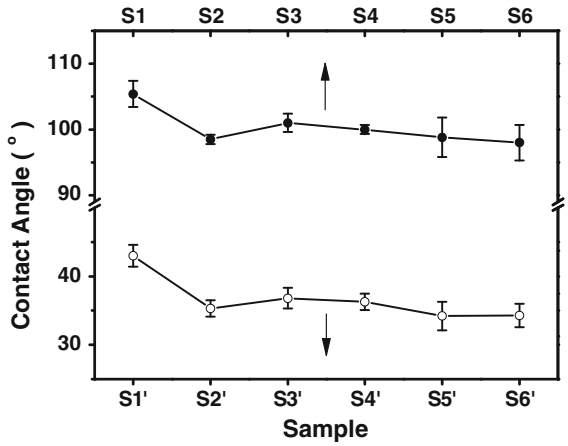

Fig. 5 Water contact angles of the CA composite scaffolds and the deacetylated cellulose composite scaffolds (n = 3)

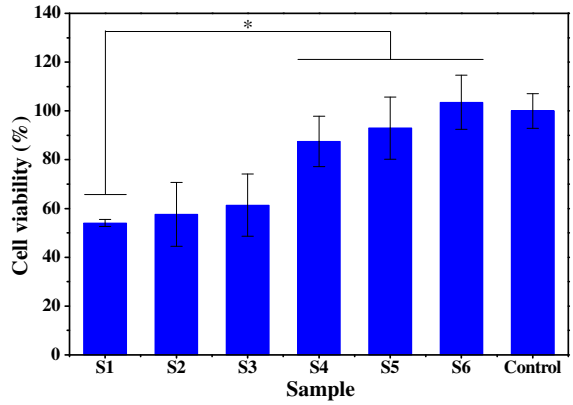

Fig. 6 Viability of VSMC after 24 h cultivation within the CA composite scaffolds. Disks (n = 3) of each sample with a diameter of 6 mm were placed in 48-well cell culture plate ($*P < 0.05$)

stained and shown in Fig. S4. VSMC status within S1 was not good. Several cells aggregated and showed small and rounded shape. After adding MCC in the scaffolds, more cells could be observed within S2. The dispersion and density of VSMC in the scaffold of S3 were getting better, and VSMC were dispersed more uniformly than S1 and S2. The results indicated that CW promoted cell attachment. For S4, not only cell density and dispersion but also the cell morphology became obviously different from S1. Some cells within S4 began to exhibit spread shape. As the content of MCC and CW increased to 7.5 and 10 wt%, cells were more abundantly dispersed throughout the scaffolds. Meanwhile, more cells performed spread morphology with increasing content of MCC and CW. Among the six scaffolds, S6 displayed the best biocompatibility, and the cells exhibited a three dimensional proliferation throughout the whole scaffold as presented in the fluorescent image. The cell adhesion and proliferation of electrospun CA scaffolds were ameliorated with the addition of MCC and CW. It might have a close relation with the surface roughness, porosity and the hydrophilicity of MCC and CW, because surface roughness and porosity of electrospun fibers has impact on cellular behaviors (Zhu et al. 2008; Luo et al. 2012). In addition, although the hydrophilicity of the entire composite film was just increased slightly, considering the microenvironment, the spots where MCC and CW were decorated should be more hydrophilic.

Scanning electron microscope images of the cultivation of VSMC within the scaffolds for 2 days are shown in Fig. 8. Merely some rounded and small cells could be found within the scaffold S1. However, some spread cells could be found in the biocomposite scaffolds. For example, cells grew along the fiber and had spread morphology in S2. Within S3, many cells were better dispersed on the scaffolds but only some spindle-shaped cells could be observed. By careful examination of S2 and S3, the actions of MCC and CW can be well interpreted. MCC was advantageous for the cell growth while CW played an important role in cell attachment. The difference could be attributed to the size of MCC and CW. The prepared MCC particles were about 20 μm length and 5 μm width, which could increase surface roughness and provide anchors for VSMC growth and proliferation (Li et al. 2013). Owing to the nanoscale dimension and high surface area, CW could be more widely dispersed in the CA fibers than MCC, and consequently meliorated cell adhesion on CA fibers. Therefore, more VSMC were attached to the fibrous scaffold dispersively. The consequences of S4, S5 and S6 were derived from the combination of the beneficial effects of MCC and CW. The biocomposite scaffolds with both MCC and CW exhibited micro-, submicro- and nano-structures; this multi-scaled feature could better mimic the biological matrix and help to improve the cell attachment and proliferation at the same time. The increased porosity also accounted for the improved cellular migration and infiltration, as well as growth and proliferation within the scaffolds.

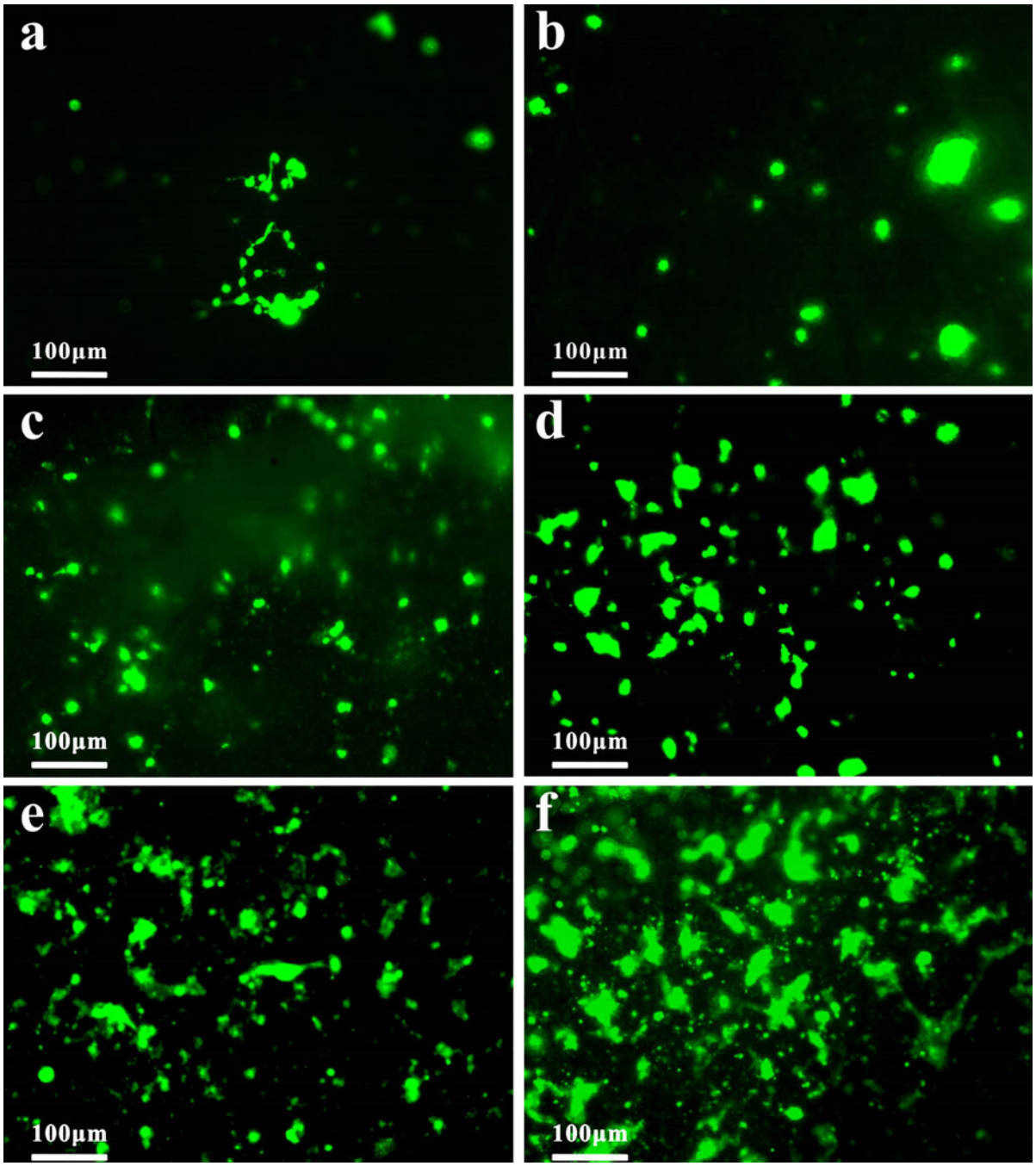

Fig. 7 Fluorescent micrographs of cells within the scaffolds of **a** S1, **b** S2, **c** S3, **d** S4, **e** S5 and **f** S6 after 2 days of cultivation

Cell viability of the deacetylated electrospun scaffolds

To further understand the roles of MCC and CW, the CA biocomposite scaffolds were hydrolyzed in 0.05 M NaOH/ethanol to obtain deacetylated cellulose composite scaffolds. As shown in Fig. 4b, the characteristic peaks of the carboxylate group nearly vanished, which was the substantial evidence of successful deacetylation. The surface morphology of

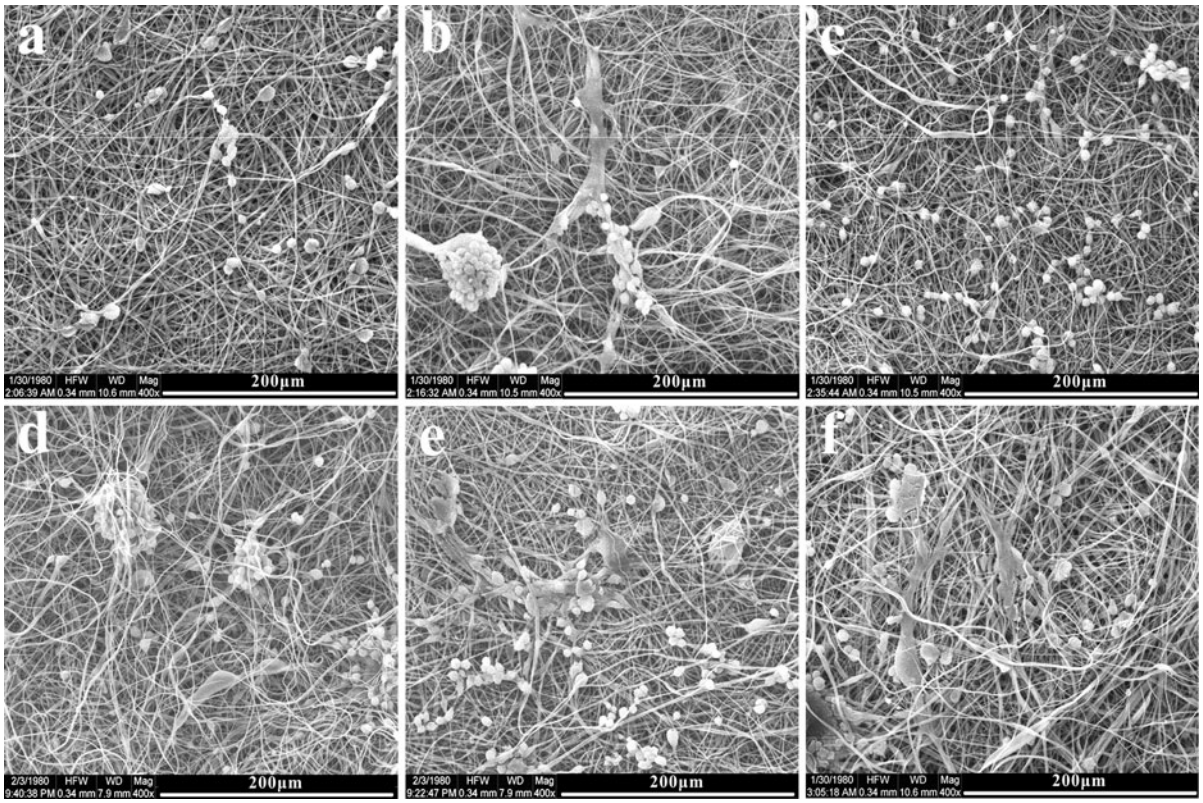

Fig. 8 SEM images of VSMC cultured within the CA composite scaffolds of **a** S1, **b** S2, **c** S3, **d** S4, **e** S5 and **f** S6 for 2 days (*Scale bar* is 200 μm)

deacetylated fibers did not exhibit obvious difference in Figs. 2 and 9. The deacetylated scaffolds became hydrophilic because CA has been changed to cellulose, and the water contact angles were in the range of 35–43° (Fig. 5). The variance tendency of water contact angles of S1′–S6′ was very close to S1–S6. MCC still proved more obvious action than CW on improving the hydrophilicity. The results further proved that the roughness and porosity of fibrous scaffolds derived from MCC and CW played an important role in the hydrophilicity of the scaffolds.

Figure 10 shows the VSMC viability within the deacetylated electrospun scaffolds determined by MTT assay. The deacetylated cellulose scaffolds possessed better biocompatibility than the CA composite scaffolds. Moreover, the scaffolds containing MCC and CW (S4′–S6′) still showed better biocompatibility than the pure cellulose scaffold (S1′), and the cell viability increased with increasing content of MCC and CW. In consideration of the slight difference in wettability of MCC, CW and hydrolyzed scaffolds, the change in hydrophilicity was not the foremost reason for this dramatic improvement. The multi-scaled structure (Kim et al. 2010), surface roughness and increased porosity derived from adding MCC and CW should be the major influence that affect cell attachment and spreading. MCC and CW exhibited arrestingly synergistic effect on cell adhesion, dispersion and proliferation. We believe the cellulose-based biocomposite scaffold with enhanced biocompatibility could extend the prospects of potential applications of natural materials in vascular tissue engineering. And the promotive effect of MCC and CW on biomaterial activity for electrospun scaffolds should be helpful for other kinds of synthetic polymers such as PCL, PLGA etc.

Conclusions

Cellulose acetate and cellulose scaffolds containing MCC and CW were successfully prepared through electrospinning and deacetylation. By introducing the

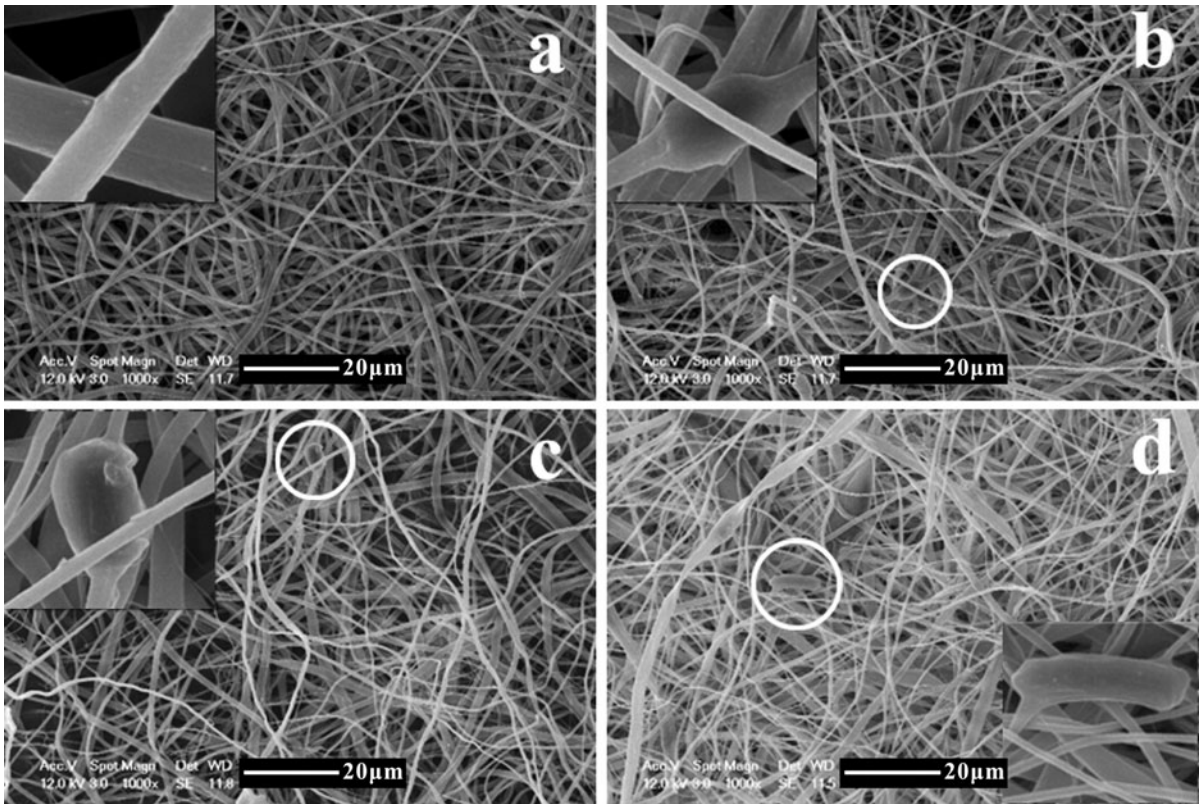

Fig. 9 SEM images of the deacetylated cellulose composite scaffolds: **a** S1′, **b** S4′, **c** S5′ and **d** S6′ (*Scale bar* is 20 μm)

micro- and nano-scaled cellulose particulates, the composite scaffolds exhibited multi-scaled organization which was more resemble to natural extracellular matrix. MCC and CW showed different effects on the electrospun fibers. For the scaffolds containing MCC, the fiber diameter distribution became widened, and the fiber surface became obviously rougher. CW stabilized the electrospinning process, and the electrospun fibers became more uniform. MCC and CW provided slightly difference on the hydrophilicity of the scaffolds. The scaffolds with MCC became more hydrophilic than CW. Vascular smooth muscle cell viability within the electrospun scaffolds containing both MCC and CW was considerably improved compared to CA and those with only MCC or CW. MCC provided anchors for cells to grow within the scaffolds, and CW ameliorated the cell adhesion for its wide dispersion. Both cell density and morphology were getting better because of the synergistic effect of MCC and CW. After deacetylation, the cellulose composite scaffolds exhibited the similar trend on both hydrophilicity and biocompatibility. The synergistic effects suggest that the cellulose particulates are promising additives to improve the biocompatibility of scaffolds for the vascular tissue engineering.

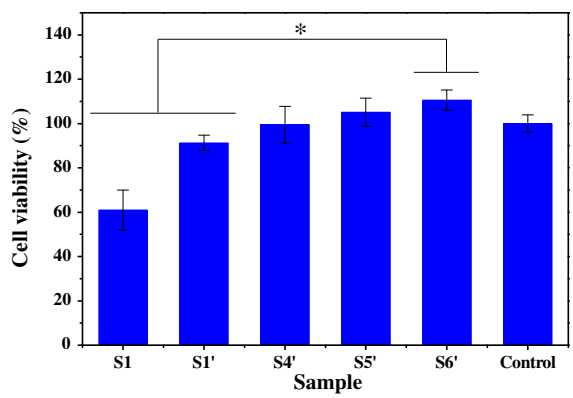

Fig. 10 VSMC viability after 24 h cultivation within the deacetylated cellulose composite scaffolds determined by MTT assay (*$P < 0.05$)

Acknowledgments This work was financially supported by National Natural Science Foundation of China (50973085 and 51273151), the Program for New Century Excellent Talents in University (NCET-11-0415), National Basic Research Program of China (973 Program, 2010CB732203) and Fundamental Research Funds for the Central Universities. Prof. Rajulu thanks the Council of Scientific and Industrial Research (CSIR) of India for the award of an Emeritus Scientist scheme, and Dr. Zhou thanks the Japan Society for the Promotion of Science (JSPS) Invitation Fellowship for Research in Japan for the financial support.

References

Araki J, Wada M, Kuga S, Okano T (1998) Flow properties of microcrystalline cellulose suspension prepared by acid treatment of native cellulose. Colloids Surf A 142:75–82

Bhattacharya M, Malinen MM, Lauren P, Lou Y-R, Kuisma SW, Kanninen L et al (2012) Nanofibrillar cellulose hydrogel promotes three-dimensional liver cell culture. J Controlled Release 164:291–298

Chakraborty A, Sain M, Kortschot M (2005) Cellulose microfibrils: a novel method of preparation using high shear refining and cryocrushing. Holzforschung 59:102–107

Coburn JM, Gibson M, Monagle S, Patterson Z, Elisseeff JH (2012) Bioinspired nanofibers support chondrogenesis for articular cartilage repair. PANS 109:10012–10017

Das K, Ray D, Bandyopadhyay NR, Ghosh T, Mohanty AK, Misra M (2009) A study of the mechanical, thermal and morphological properties of microcrystalline cellulose particles prepared from cotton slivers using different acid concentrations. Cellulose 16:783–793

Deitzel J, Kleinmeyer J, Harris D, Beck Tan N (2001) The effect of processing variables on the morphology of electrospun nanofibers and textiles. Polymer 42:261–272

Dong S, Hirani AA, Colacino KR, Lee YW, Roman M (2012) Cytotoxicity and cellular uptake of cellulose nanocrystals. Nano Life 02:1241006–1241017

Du J, Hsieh YL (2009) Cellulose/chitosan hybrid nanofibers from electrospinning of their ester derivatives. Cellulose 16:247–260

Dugan JM, Gough JE, Eichhorn SJ (2010) Directing the morphology and differentiation of skeletal muscle cells using oriented cellulose nanowhiskers. Biomacromolecules 11:2498–2504

Dugan JM, Collins RF, Gough JE, Eichhorn SJ (2013) Oriented surfaces of adsorbed cellulose nanowhiskers promote skeletal muscle myogenesis. Acta Biomater 9:4707–4715

Eldessouki M, Buschle-Diller G, Gowayed Y (2011) Poly (L-lysine)/microcrystalline cellulose biocomposites for porous scaffolds. Polym Compos 32:1937–1944

Favier V, Chanzy H, Cavaille JY (1995) Polymer nanocomposites reinforced by cellulose whiskers. Macromolecules 28:6365–6367

Gouma P, Ramachandran K, Firat M, Connolly M, Zuckermann R, Balaszi C et al (2010) Novel bioceramics for bone implants. In: Narayan R, Colombo P (eds) Advances in bioceramics and porous ceramics, vol II. Wiley, Hoboken, pp 35–44

Hoffman AS (2012) Hydrogels for biomedical applications. Adv Drug Deliv Rev 64:18–23

Ilharco L, de Barros RB (2000) Aggregation of pseudoisocyanine iodide in cellulose acetate films: structural characterization by FTIR. Langmuir 16:9331–9337

Kakisis JD, Liapis CD, Breuer C, Sumpio BE (2005) Artificial blood vessel: the Holy Grail of peripheral vascular surgery. J Vasc Surg 41:349–354

Khademhosseini A, Eng G, Yeh J, Fukuda J, Blumling J III, Langer R et al (2006) Micromolding of photocrosslinkable hyaluronic acid for cell encapsulation and entrapment. J Biomed Mater Res A 79A:522–532

Kim SJ, Jang DH, Park WH, Min BM (2010) Fabrication and characterization of 3-dimensional PLGA nanofiber/microfiber composite scaffolds. Polymer 51:1320–1327

Klemm D, Heublein B, Fink H-P, Bohn A (2005) Cellulose: fascinating biopolymer and sustainable raw material. Angew Chem Int Ed 44:3358–3393

Ladd MR, Lee SJ, Stitzel JD, Atala A, Yoo JJ (2011) Co-electrospun dual scaffolding system with potential for muscle-tendon junction tissue engineering. Biomaterials 32:1549–1559

Li W, Wang R, Liu S (2011) Nanocrystalline cellulose prepared from softwood karft pulp via ultrasonic-assisted acid hydrolysis. BioResources 6:4271–4281

Li J, Li Y, Liu X, Zhang J, Zhang Y (2013) Strategy to introduce an hydroxyapatite-keratin nanocomposite into a fibrous membrane for bone tissue engineering. J Mater Chem B 1:432–437

Liu H, Hsieh YL (2002) Ultrafine fibrous cellulose membranes from electrospinning of cellulose acetate. J Polym Sci, Part B: Polym Phys 40:2119–2129

Luo C, Li L, Shi X, Yang G, Ding S, Zhi W et al (2012) Modulating cellular behaviors through surface nanoroughness. J Mater Chem 22:15654–15664

Ma Z, He W, Yong T, Ramakrishna S (2005) Grafting of gelatin on electrospun poly (caprolactone) nanofibers to improve endothelial cell spreading and proliferation and to control cell orientation. Tissue Eng 11:1149–1158

Male KB, Leung ACW, Montes J, Kamen A, Luong JHT (2012) Probing inhibitory effects of nanocrystalline cellulose: inhibition versus surface charge. Nanoscale 4:1373–1379

Moon RJ, Martini A, Nairn J, Simonsen J, Youngblood J (2011) Cellulose nanomaterials review: structure, properties and nanocomposites. Chem Soc Rev 40:3941–3994

Müller FA, Müller L, Hofmann I, Greil P, Wenzel MM, Staudenmaier R (2006) Cellulose-based scaffold materials for cartilage tissue engineering. Biomaterials 27:3955–3963

Pooyan P, Tannenbaum R, Garmestani H (2012) Mechanical behavior of a cellulose-reinforced scaffold in vascular tissue engineering. J Mech Behav Biomed Mater 7:50–59

Rnjak-Kovacina J, Wise SG, Li Z, Maitz PKM, Young CJ, Wang Y et al (2011) Tailoring the porosity and pore size of electrospun synthetic human elastin scaffolds for dermal tissue engineering. Biomaterials 32:6729–6736

Rodríguez K, Gatenholm P, Renneckar S (2012) Electrospinning cellulosic nanofibers for biomedical applications: structure and in vitro biocompatibility. Cellulose 19: 1583–1598

Shopsowitz KE, Hamad WY, MacLachlan MJ (2011) Chiral nematic mesoporous carbon derived from nanocrystalline cellulose. Angew Chem Int Ed 50:10991–10995

Son WK, Youk JH, Lee TS, Park WH (2004a) Electrospinning of ultrafine cellulose acetate fibers: studies of a new solvent system and deacetylation of ultrafine cellulose acetate fibers. J Polym Sci, Part B: Polym Phys 42:5–11

Son WK, Youk JH, Lee TS, Park WH (2004b) Preparation of antimicrobial ultrafine cellulose acetate fibers with silver nanoparticles. Macromol Rapid Commun 25:1632–1637

Teo WE, Kotaki M, Mo XM, Ramakrishna S (2005) Porous tubular structures with controlled fibre orientation using a modified electrospinning method. Nanotechnology 16:918

Thibault RA, Mikos AG, Kasper FK (2013) Scaffold/extracellular matrix hybrid constructs for bone-tissue engineering. Adv Healthc Mater 2:13–24

Truong YB, Glattauer V, Briggs KL, Zappe S, Ramshaw JAM (2012) Collagen-based layer-by-layer coating on electrospun polymer scaffolds. Biomaterials 33:9198–9204

Tuzlakoglu K, Bolgen N, Salgado A, Gomes M, Piskin E, Reis R (2005) Nano- and micro-fiber combined scaffolds: a new architecture for bone tissue engineering. J Mater Sci Mater Med 16:1099–1104

Van Vlierberghe S, Dubruel P, Schacht E (2011) Biopolymer-based hydrogels as scaffolds for tissue engineering applications: a review. Biomacromolecules 12:1387–1408

Wang S, Castro R, An X, Song C, Luo Y, Shen M et al (2012) Electrospun laponite-doped poly (lactic-co-glycolic acid) nanofibers for osteogenic differentiation of human mesenchymal stem cells. J Mater Chem 22:23357–23367

Watanabe A, Morita S, Ozaki Y (2007) Temperature-dependent changes in hydrogen bonds in cellulose Iα studied by infrared spectroscopy in combination with perturbation-correlation moving-window two-dimensional correlation spectroscopy: comparison with cellulose Iβ. Biomacromolecules 8:2969–2975

Wu SC, Chang WH, Dong GC, Chen KY, Chen YS, Yao CH (2011) Cell adhesion and proliferation enhancement by gelatin nanofiber scaffolds. J Bioact Compat Polym 26:565–577

Zhao L, Mei S, Chu PK, Zhang Y, Wu Z (2010) The influence of hierarchical hybrid micro/nano-textured titanium surface with titania nanotubes on osteoblast functions. Biomaterials 31:5072–5082

Zhou C, Chu R, Wu R, Wu Q (2011) Electrospun polyethylene oxide/cellulose nanocrystal composite nanofibrous mats with homogeneous and heterogeneous microstructures. Biomacromolecules 12:2617–2625

Zhu H, Ji J, Shen J (2004) Biomacromolecules electrostatic self-assembly on 3-dimensional tissue engineering scaffold. Biomacromolecules 5:1933–1939

Zhu X, Cui W, Li X, Jin Y (2008) Electrospun fibrous mats with high porosity as potential scaffolds for skin tissue engineering. Biomacromolecules 9:1795–1801